

AIAA 81-1019R

# Multiple Solutions of the Transonic Potential Flow Equation

John Steinhoff\*

*Grumman Aerospace Corporation, Bethpage, New York*

and

Antony Jameson†

*Princeton University, Princeton, New Jersey*

The two-dimensional transonic potential flow equation, when solved in discrete form for steady flow over an airfoil, has been found to yield more than one solution in certain bands of angle of attack and Mach number. The most striking example of this is the appearance of nonsymmetric solutions with large positive or negative lift, for symmetric airfoils at zero angle of attack. The behavior of these "anomalous" solutions is examined as grid size is varied by large factors and found to be not qualitatively different from that of "normal" solutions (outside the nonuniqueness band). Thus, it appears that the effect is not due to discretization error, and that the basic transonic potential flow partial-differential equation admits nonunique solutions for certain values of angle of attack and Mach number.

## Introduction

THE full potential equation is widely used for computing transonic flow over aircraft. It expresses conservation of mass, neglecting effects due to viscosity, vorticity, and entropy production. For flow without massive separated regions, where the shocks are not too strong, the equation is a good approximation to the Navier-Stokes equations outside of a thin boundary-layer and wake region. In combination with boundary-layer methods, it has been used to give very accurate solutions for flow over airfoils in two dimensions.<sup>1</sup>

Recently, the authors discovered that in certain bands of angle of attack and Mach number, the full potential equation, when solved in discrete form for steady flow over airfoils, yields multiple solutions. These solutions have very different values of lift and drag.

The purpose of this paper is to present results of numerical experiments designed to test whether the nonuniqueness appears as a result of the discretization procedure, or whether the continuum problem admits a corresponding nonuniqueness. Even if these solutions are caused by discretization error, it may be important to know that a small perturbation can result in a very different solution.

This paper consists of three basic parts. In the first, details of the difference scheme are described. In the second, results are presented for a symmetric Joukowski airfoil at zero angle of attack ( $\alpha$ ) and fixed freestream Mach number ( $M_\infty$ ). Here, in addition to the expected symmetric solution, two (mirror-image) unsymmetric solutions appear with large absolute value of lift coefficient ( $C_L$ ). In this section we attempt to validate these solutions both by checking that boundary conditions and the Kutta condition are satisfied, and by studying the variation of the solutions as the computational grid and artificial viscosity are varied. In the third part, the behavior of the "anomalous" solutions is studied as  $M_\infty$  and  $\alpha$  are varied.

## Difference Scheme

In a curvilinear coordinate system, the full potential equation can be written<sup>2</sup>

$$\frac{\partial}{\partial X}(\rho h U) + \frac{\partial}{\partial Y}(\rho h V) = 0$$

where

$$h = \det(H)$$

The isentropic relation for the density

$$\rho = \left[ 1 + \frac{\gamma-1}{2} M_\infty^2 (1-q^2) \right]^{1/(\gamma-1)}$$

where  $q$  is the speed and  $\gamma$  the ratio of specific heats. The basic transformation from physical  $(x,y)$  to computational  $(X,Y)$  frames is expressed by the matrix

$$H = \begin{pmatrix} x_X & x_Y \\ y_X & y_Y \end{pmatrix}$$

The physical velocities are derived from a potential,  $\phi$

$$\begin{pmatrix} u \\ v \end{pmatrix} = (H^T)^{-1} \begin{pmatrix} \phi_X \\ \phi_Y \end{pmatrix} + \begin{pmatrix} u_\infty \\ v_\infty \end{pmatrix}$$

and the contravariant velocities required for the transformed flux balance equation are

$$\begin{pmatrix} U \\ V \end{pmatrix} = (H)^{-1} \begin{pmatrix} u \\ v \end{pmatrix}$$

We use the "finite volume" discretization schemes described in Ref. 2. Here, two interlocking meshes are used. On one, the potential  $\phi$  and the coordinates  $(x,y, X,Y)$  are defined and the flux balance is satisfied (at convergence). On the other, which coincides with the cell centers of the first, the density and velocities are defined.

Except for one case computed with a parabolic mapping, all of our calculations use an "O" type grid. A Joukowski transformation is used to map the airfoil to a near circle which is then mapped to a circle by a shearing transformation (for a Joukowski airfoil this shearing is not needed).

A stretching and inversion are then used

$$R' = [\Delta + (1-\Delta)\Delta]^{-1}$$

Presented as Paper 81-1019 at the AIAA Fifth Computational Fluid Dynamics Conference, Palo Alto, Calif., June 22-23, 1981; submitted July 6, 1981; revision received Feb. 22, 1982. Copyright © American Institute of Aeronautics and Astronautics, Inc., 1981. All rights reserved.

\*Staff Scientist; presently, Associate Professor, Department of Engineering Science and Mechanics, University of Tennessee Space Institute, Tullahoma, Tenn. Member AIAA.

†Professor, Department of Mechanical and Aerospace Engineering.

where  $R'$  is the radius of a point in the initial mapped plane,  $R$  the radius in the computational plane, and  $\Delta$  a small parameter which controls the far field boundary.

The compressible vortex solution

$$\phi_F = (\Gamma/2\pi) \tan^{-1}(\beta \tan \theta) \quad \beta = (1 - M_\infty^2)^{1/2} \quad (1)$$

is used for the far field boundary conditions, where  $\Gamma$  is the value of the circulation. The requirement that there be no flow around the trailing edge determines  $\Gamma$ .

The calculation of the supersonic zone is stabilized by the addition of artificial viscosity to provide an upwind bias. This has the form

$$P_{i+1/2,j} - P_{i-1/2,j} + Q_{i,j+1/2} - Q_{i,j-1/2}$$

where  $P$  and  $Q$  are defined as follows.

A switching function is defined:

$$\mu = \max(0, 1 - M_c^2/M^2)$$

This vanishes when the local Mach number  $M$  is less than a cutoff  $M_c$ . Also, let

$$\tilde{P} = \rho h \frac{\mu}{a^2} \left( U^2 \frac{\partial^2}{\partial X^2} + UV \frac{\partial^2}{\partial X \partial Y} \right) \phi$$

$$\tilde{Q} = \rho h \frac{\mu}{a^2} \left( UV \frac{\partial^2}{\partial X \partial Y} + V^2 \frac{\partial^2}{\partial Y^2} \right) \phi$$

Then,

$$P_{i+1/2,j} = \tilde{P}_{i,j} - \epsilon_{ij} \tilde{P}_{i-1,j} \quad (U > 0)$$

$$P_{i+1/2,j} = \epsilon_{i+1,j} \tilde{P}_{i+2,j} - \tilde{P}_{i+1,j} \quad (U < 0)$$

with corresponding formulas for  $Q_{i,j+1/2}$ .

If the coefficient  $\epsilon = 1 - 0(\Delta X)$ , then  $P = 0(\Delta X)$  and the added terms are  $0(\Delta X^2)$ , since the difference in  $P$  is not divided by  $\Delta X$ . Accordingly, this coefficient is defined

$$\epsilon_{i,j} = \max(0, 1 - \lambda(\rho_{i+1/2,j} - \rho_{i-1/2,j}))$$

The density difference acts as a shock detector, causing the scheme to revert to a first-order accurate form near a shock wave. In the calculations presented in this paper, the artificial viscosity is cut off at Mach number  $M_c \sim 0.8$ . (Essentially the same results have been obtained with  $M_c = 0.95$  and above. Due to the second-order accuracy of the viscosity term the solution is not sensitive to this switching value. Faster convergence, however, is obtained with the lower value of  $M_c$ .)

A multigrid-approximate factorization scheme<sup>3</sup> is used to solve the discrete equations. This provides strong damping for error components in all frequency bands and allows us to converge to machine accuracy, if desired. The far field boundary conditions are updated to allow for changes of circulation after each iteration on each grid.

### Multiple Solutions

Figures 1 and 2 show the pressure distribution ( $C_p$ ) over the upper and lower surfaces for two alternative solutions of the flow past an 11.8% thick Joukowski airfoil at a Mach number of 0.832 and zero angle of attack. One solution is symmetric, as expected. The other is unsymmetric, with the shock wave on the upper surface displaced rearward to a point near but not at the trailing edge, and the shock wave on the lower surface displaced forward. The lift coefficient  $C_L$  is +0.5544 for this unsymmetric solution and there is a corresponding mirror image solution with a lift coefficient of -0.5544. The grid for these calculations was an "O" mesh, depicted in Fig. 3, with 256 cells around the airfoil and 64 cells

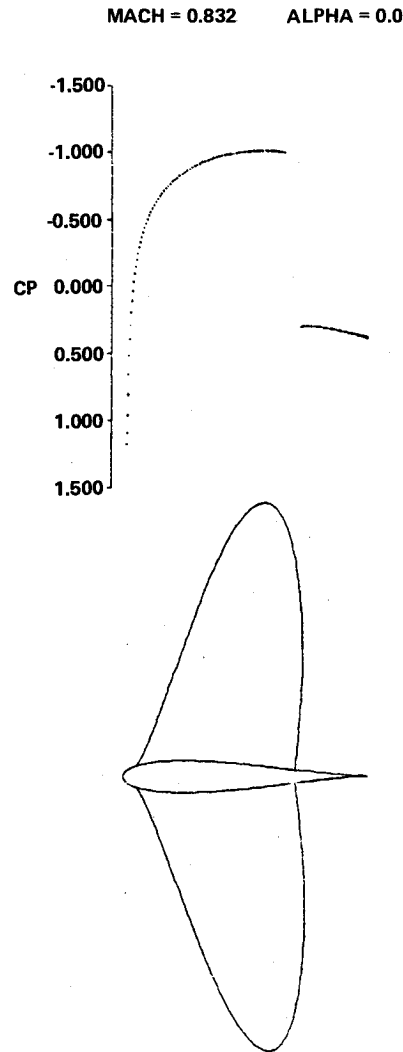


Fig. 1 Symmetric solution.

between the airfoil and the outer boundary. (Only the inner portion of the grid is pictured, the actual outer boundary is smooth.)

The first test made on the anomalous solutions was that they accurately satisfy the difference equations. The decay of the average residual for this grid and a similar solution on a  $128 \times 32$  grid is plotted in Fig. 4. The multigrid scheme will converge to machine accuracy, and there is no doubt that the difference equations are satisfied. Tests were made to verify that the same code would converge to either the  $+C_L$ , the  $-C_L$ , or the symmetric solution if the code is started close enough to each.

The next check was to verify that the far field boundary conditions are properly satisfied. With the freestream subtracted out, these are Dirichlet conditions corresponding to a compressible vortex [Eq. (1)]. The computed solution was found to decay smoothly in the far field like a vortex and doublet in a uniform stream at zero angle of attack, as expected. As a further check, the distance to the outer boundary was reduced from 25 chords to 8 chords by reducing the grid stretching. This caused only a 5% change (increase) in the lift coefficient.

Another check on these solutions concerned the Kutta condition. The pressures on the upper and lower surfaces smoothly went to the same value at the trailing edge and the streamline left the trailing edge smoothly.

The final test was to verify the convergence of the solution with grid refinement. In Fig. 5, values of  $C_L$  are plotted for the unsymmetric solution on grids with  $96 \times 24$ ,  $128 \times 32$ ,

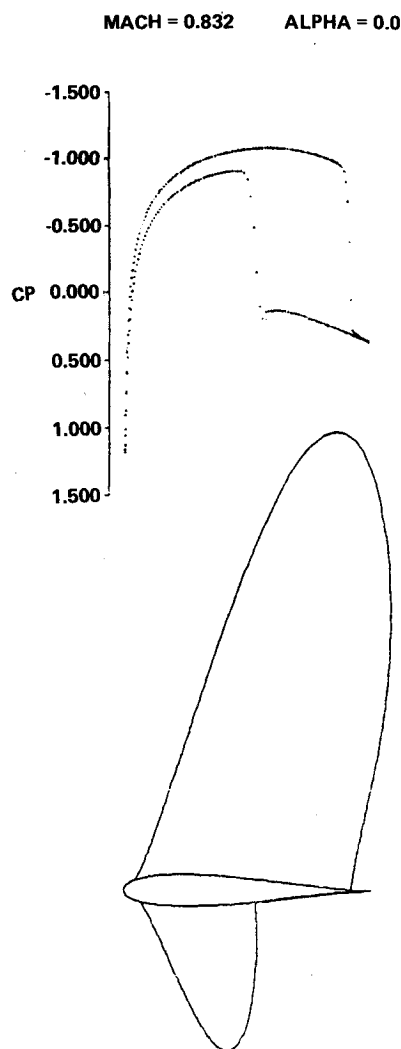


Fig. 2 Unsymmetric solution.

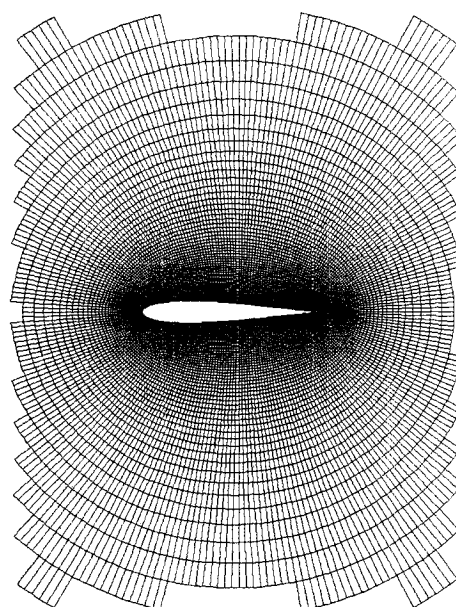


Fig. 3 Computational grid.

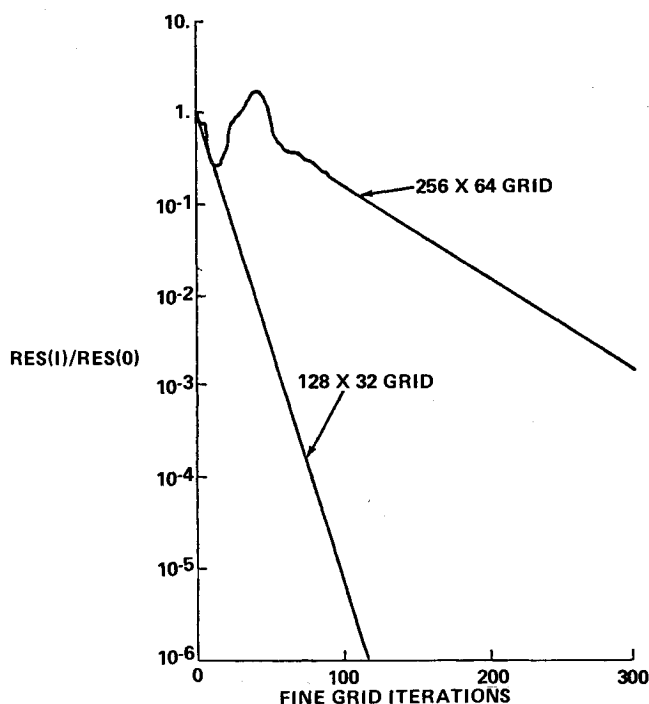


Fig. 4 Residual decay.

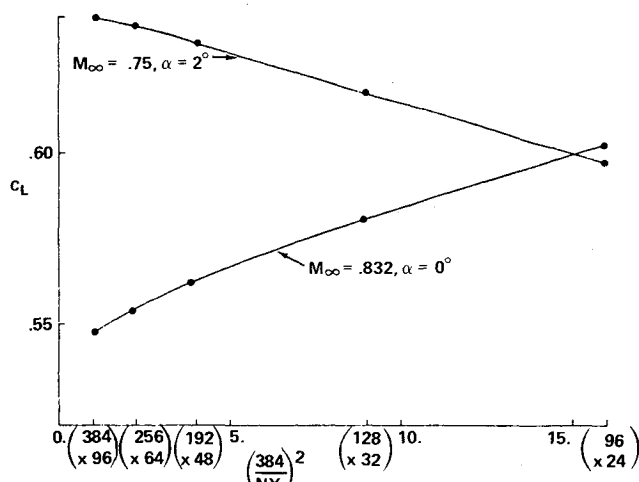


Fig. 5 Lift convergence.

192  $\times$  48, 256  $\times$  64, and 384  $\times$  192 cells. For comparison,  $C_L$  is also plotted for the same airfoil at  $M_\infty = 0.75$ ,  $\alpha = 2^\circ$ , where only one solution was found. It can be seen that  $C_L$  converges at comparable rates for the two solutions. The reason that  $C_L$  decreased as the grid was refined for the  $\alpha = 0$  solution was that the lower shock, which was weaker than the upper one, became stronger and moved backward, increasing the magnitude of the negative contribution of the lower part of the airfoil to  $C_L$ . The upper shock did not change as much as the grid was refined. For the  $\alpha = 2^\circ$  case, there was only a single shock located at the upper surface, which moved backward as the grid was refined.

The artificial viscosity in these calculations had the second-order form defined in the previous section. It was verified that the unsymmetric solutions could also be obtained with the first-order accurate form of artificial viscosity obtained by setting  $\epsilon = 0$ .

In order to check whether the solution is a peculiarity depending on the form of the grid, calculations were also performed on a "C" mesh generated by mapping to parabolic coordinates. The solution is displayed in Fig. 6 for a grid with 128  $\times$  32 cells. With this type of mesh, the cell width near the trailing edge was 400 times the width on the 256  $\times$  64 "O" mesh. It can be seen that the unsymmetric solution persists.

### Hysteresis

The unsymmetric solutions have been found only in a narrow Mach number band. In the case of the 11.8% thick Joukowski airfoil at zero angle of attack, only the symmetric solution could be found below 0.82 and above 0.85. The lift

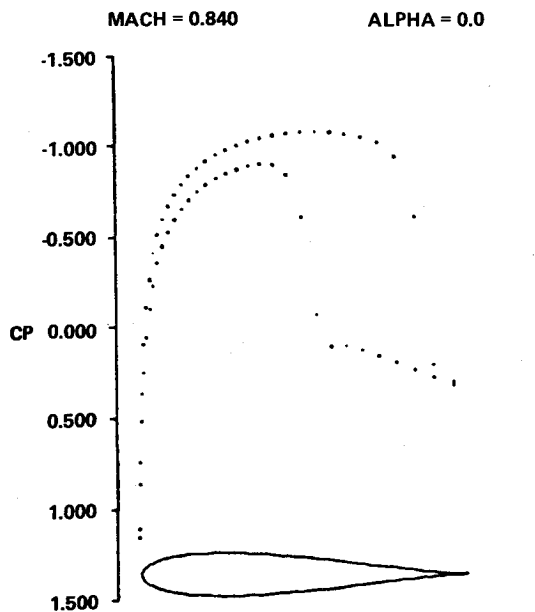


Fig. 6 Unsymmetric solution parabolic coordinates.

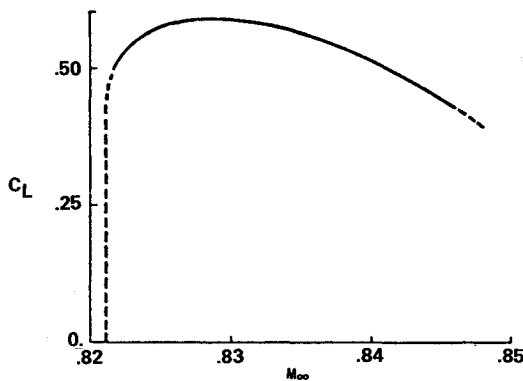
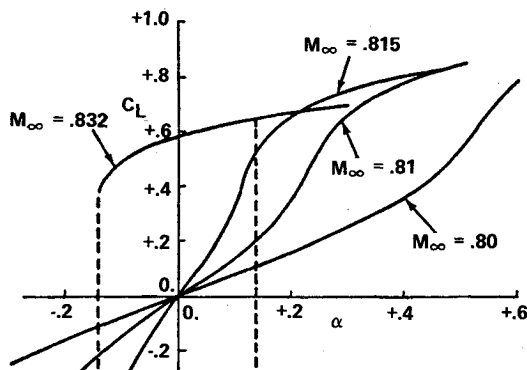
Fig. 7 Unsymmetric solution  $\alpha = 0$ .

Fig. 8 Hysteresis Joukowski airfoil.

coefficient for the unsymmetric solution at  $\alpha = 0$  is plotted in Fig. 7 for Mach numbers between these limits. In this band the nonuniqueness was associated with a hysteresis. In Fig. 8,  $C_L$  as a function of  $\alpha$  is plotted for a series of Mach numbers. The curves for Mach number less than 0.82 show the expected behavior. Above 0.82, on the other hand, we find the hysteresis. On the 0.832 Mach number curve, the two intercepts of the  $C_L$  axis at  $\alpha = 0$  correspond to the two unsymmetric solutions discussed in the previous section. Starting from the upper right-hand part of this curve, which corresponds to the upper shock being close to the trailing edge, we can generate the rest of the curve by incrementally decreasing  $\alpha$  and, at each step, computing a new solution

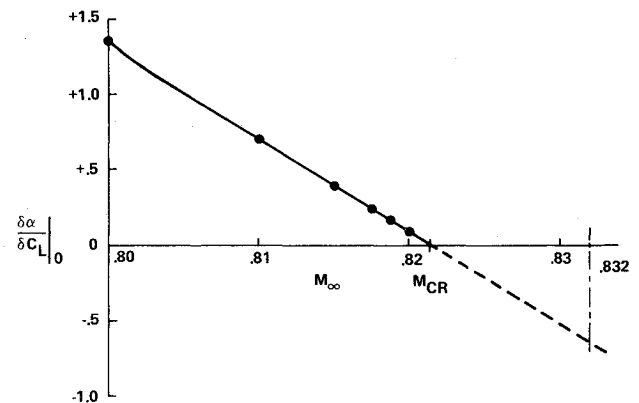
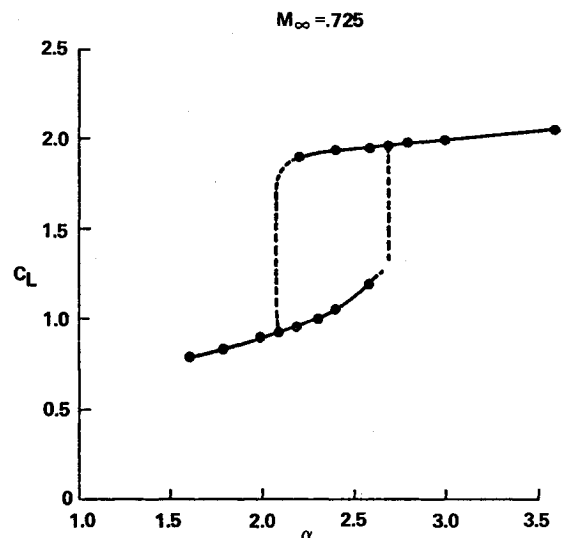
Fig. 9 Determination of  $M_{crit}$ .

Fig. 10 Hysteresis RAE 2822 airfoil.

from the previous one. Once we decrease  $\alpha$  below about  $-0.14$  deg the solution "flips" to the negative  $C_L$  one. We can then generate this part of the curve in the same way. The symmetric solution ( $C_L = 0$ ,  $\alpha = 0$ ) proved to be unstable to small perturbations, and went over to either the positive or negative  $C_L$  ( $\alpha = 0$ ) solution.

Below the Mach number where hysteresis appears, it can be seen that the change in  $C_L$  for a small change in  $\alpha$  at  $\alpha = 0$  increases as we increase  $M_\infty$  and becomes large as we approach a critical value  $M_{crit}$ .

Thinking of  $\alpha$  as a function of  $C_L$ , the slope of  $\alpha$  vs  $C_L$  at  $C_L = 0$  goes smoothly to zero at  $M_{crit}$ , and apparently becomes negative beyond  $M_{crit}$ , where the hysteresis is found. This can be seen in Fig. 9 where this quantity is plotted for a series of Mach numbers. The extrapolated negative slope value at Mach 0.832 is consistent with the hysteresis curve of Fig. 8. An unstable branch with this extrapolated slope, if included with the stable positive slope branches pictured, would result in a continuous S-shaped curve for the locus of possible solutions.

The hysteresis occurs in a rather narrow band of angle of attack. If this band were to become smaller as the mesh was refined, there is a possibility that instead of a nonunique solution there would be a rapid switch from large negative to large positive  $C_L$  as the angle of attack passed through zero. However, refinement of the mesh did not indicate any significant narrowing of the band. Its width was also insensitive to the far field stretching and placement of the outer boundary. Also, the value of  $M_{crit}$  was not sensitive to mesh refinement or far field stretching.

A final result is presented in Fig. 10. Values of  $C_L$  vs  $\alpha$  for an RAE 2822 airfoil at 0.725 Mach number were computed

using a "C" mesh with the first-order form of artificial viscosity. A similar hysteresis band can be seen. We have also found similar results for an NYU 82-06-09 airfoil. Here, a conservative finite difference rather than finite volume scheme was used.

### Conclusions

Multiple solutions of the discrete full potential equation have been found for steady two-dimensional flow over airfoils. The most striking example is the appearance of unsymmetric solutions with large positive or negative values of lift for a symmetric airfoil at zero angle of attack. This occurs only in a narrow band of Mach number, between 0.82 and 0.85 in the case of an 11.8% thick Joukowski airfoil.

Extensive numerical experiments, including the use of alternative grids and extreme grid refinement, have confirmed the persistence of these solutions. Hence, it appears likely that they actually correspond to a nonuniqueness of the continuum problem, and are not a consequence of discretization error. Since the rearward shock wave in the unsymmetric solution is not quite at the trailing edge, it seems that the nonuniqueness is not caused by interference between a shock wave at the trailing edge and the Kutta condition.

The multiple solutions may have a physical counterpart. The Mach number band in which they appear is just the band in which an airfoil of this thickness typically experiences buffeting, with the upper and lower shocks alternately

reaching a forward and rearward position similar to our positive and negative lift solutions. While buffeting may be triggered by boundary-layer separation, this raises the question of whether an instability of the outer inviscid part of the flow may also be a contributing factor to this phenomenon.

The nonunique solutions were found by a sophisticated iterative method, and it is not known whether they correspond to stable equilibrium points of the true time-dependent equation. Also, it is not known whether they are only associated with the potential flow approximation, or whether a similar nonuniqueness can also occur in solutions to the Euler or Navier-Stokes equations. An investigation of these questions would shed more light on the possible physical significance of this phenomenon.

### References

- <sup>1</sup>Melnik, R. W., Chow, R., and Mead, H. R., "Theory of Viscous Transonic Flow over Airfoils at High Reynolds Number," AIAA Paper 7-680, 1977.
- <sup>2</sup>Jameson, A. and Caughey, D. A., "A Finite Volume Method for Transonic Potential Flow Calculations," *Proceedings of AIAA 3rd Computational Fluid Dynamics Conference*, Albuquerque, N. Mex., June 1977, pp. 35-54.
- <sup>3</sup>Jameson, A., "A Multi-Grid Scheme for Transonic Potential Calculations on Arbitrary Transonic Potential Calculations on Arbitrary Grids," *Proceedings of AIAA 4th Computational Fluid Dynamics Conference*, Williamsburg, Va., July 1979, pp. 122-146.

## *From the AIAA Progress in Astronautics and Aeronautics Series . . .*

# VISCOUS FLOW DRAG REDUCTION—v. 72

*Edited by Gary R. Hough, Vought Advanced Technology Center*

One of the most important goals of modern fluid dynamics is the achievement of high speed flight with the least possible expenditure of fuel. Under today's conditions of high fuel costs, the emphasis on energy conservation and on fuel economy has become especially important in civil air transportation. An important path toward these goals lies in the direction of drag reduction, the theme of this book. Historically, the reduction of drag has been achieved by means of better understanding and better control of the boundary layer, including the separation region and the wake of the body. In recent years it has become apparent that, together with the fluid-mechanical approach, it is important to understand the physics of fluids at the smallest dimensions, in fact, at the molecular level. More and more, physicists are joining with fluid dynamicists in the quest for understanding of such phenomena as the origins of turbulence and the nature of fluid-surface interaction. In the field of underwater motion, this has led to extensive study of the role of high molecular weight additives in reducing skin friction and in controlling boundary layer transition, with beneficial effects on the drag of submerged bodies. This entire range of topics is covered by the papers in this volume, offering the aerodynamicist and the hydrodynamicist new basic knowledge of the phenomena to be mastered in order to reduce the drag of a vehicle.

*456 pp., 6 × 9, illus., \$25.00 Mem., \$40.00 List*

TO ORDER WRITE: Publications Dept., AIAA, 1290 Avenue of the Americas, New York, N.Y. 10104